Electronic Supplementary Information (ESI):

Water-Enhanced CO_2 Capture with Molecular Salt Sodium Guanidinate

Hayden A. Evans,[1*] *Marcus Carter,*[1] *Wei Zhou,*[1] *Taner Yildirim,*[1] *Craig M. Brown,*[1,2] *Hui Wu*[1]*

[1]NIST Center for Neutron Research, National Institute of Standards and Technology, Gaithersburg, Maryland 20899-6102United States;

[2] Department of Chemical and Biomolecular Engineering, University of Delaware, Newark, Delaware 19716, United States.

Email: hayden.evans@nist.gov; huiwu@nist.gov

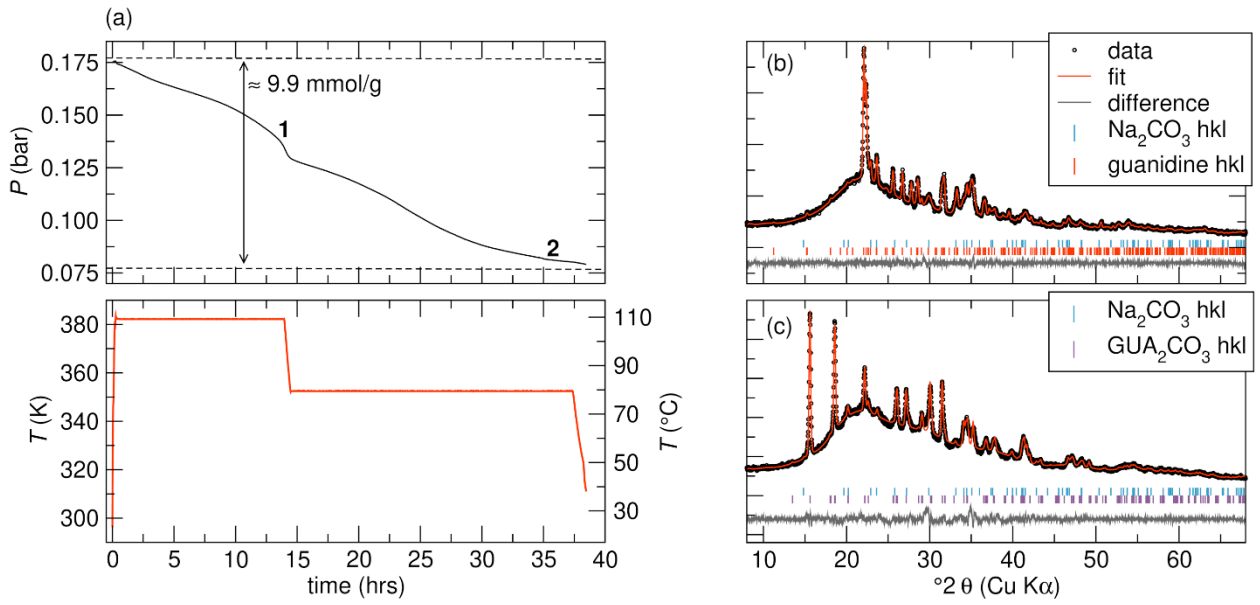

Fig. S1. (a) (top) CO_2 absorption change profile with an initial ≈ 0.1 bar CO_2 pressure and the (bottom) tested temperature range of $NaCN_3H_4$. Temperature was intentional reduced after induction to minimize the unwanted side reactions from the unstable intermediates under low CO_2 pressure and static humidity-limit condition (see more explanation in Fig. S16); b) and c) PXRD Pawley fitting results of the products collected at the end of induction (b) (Monoclinic Na_2CO_3, Space group 12, a = 8.915(7) Å b = 5.249(6) Å c = 6.064(3) Å, β = 99.87(9)°. Orthorhombic guanidine, space group 61, a = 8.561(2) Å b = 9.210(2) Å c = 15.746(5) Å) and after the complete reaction. (c) (labeled as stage "**1**" and "**2**" in top panel (a), respectively) (Tetragonal guanidinium carbonate (labeled as GUA_2CO_3 in Fig.), space group 92, $a = b$ = 6.960(1), c = 19.567(4). Monoclinic Na_2CO_3, Space group 12, a = 8.900(2) Å, b = 5.214(2) Å, c = 6.045(2) Å, β = 100.70(3)°.) The products after final absorption with an initial 0.1 bar CO_2 pressure appear the same as those observed after final absorption with an initial 1 bar CO_2 pressure.

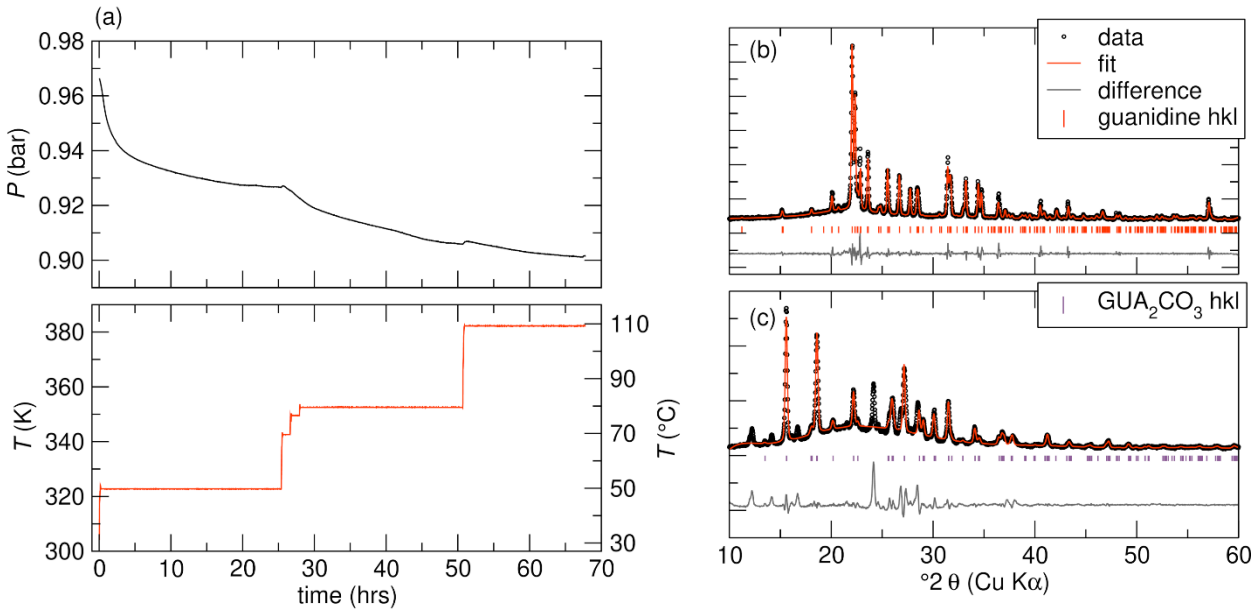

Fig. S2. a) (top) CO_2 absorption change profile with an initial ≈ 1.0 bar CO_2 pressure and the (bottom) tested temperature range of guanidine (CN_3H_5); b) The Pawley fit XRD pattern of the initial pristine guanidine CN_3H_5 (Orthorhombic guanidine, space group 61, a = 8.581(1) Å b = 9.219(1) Å c = 15.776(2) Å) and (c) Pawley fit of the final product after chemisorption with CO_2 shown in a) (Tetragonal guanidinium carbonate (labeled as GUA_2CO_3 in Fig.), space group 92, a = b = 6.960(1), c = 19.567(4)). The XRD pattern of the chemisorption product shows extra peaks from unknown phases besides $(CN_3H_6)_2CO_3$, indicating possible side reactions occurring during absorption. Compared to $NaCN_3H_4$, the bulk guanidine shows rather sluggish reaction with CO_2 with the formation of unknown impurity phase(s) from possible side reactions accompanied. Therefore, we expect that the guanidine formed during the induction of $NaCN_3H_4$ should be in the form of many small crystallites or droplets embedded evenly throughout the sample because of the progressive spreading of H_2O. Such small size guanidine crystallites/droplets would presumably help improve kinetics upon reacting with CO_2 in terms of the reduced diffusion distances and increased accessibility of CO_2 reaction sites. This might also contribute to the rapid absorption after the induction.

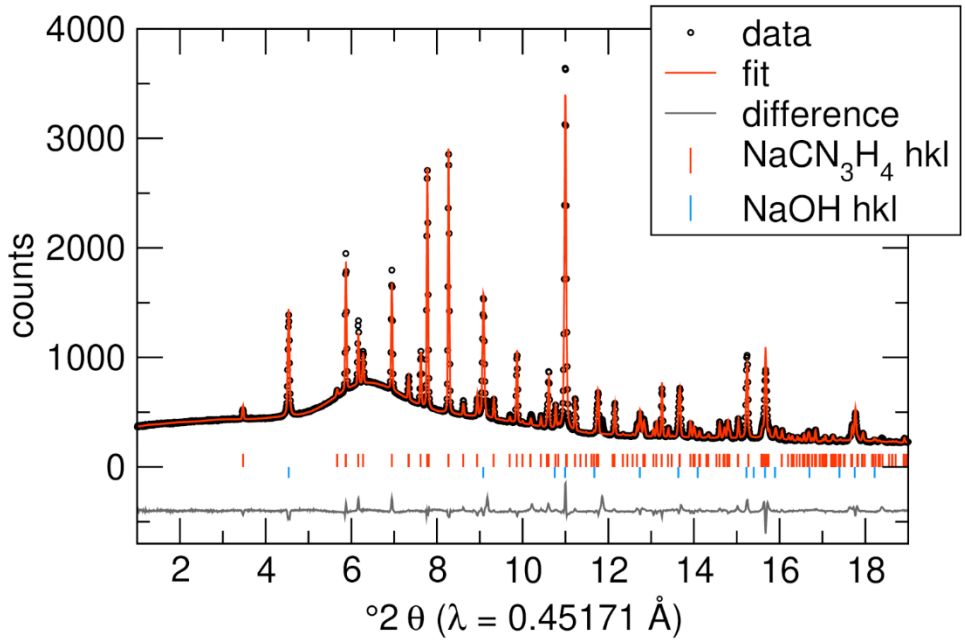

Fig S3. Representative Rietveld refinement fit of X-ray powder diffraction data of $NaCN_3H_4$ under static limited humidity CO_2 after 0.10 hours, 330 K [APS, 17-BM]. R_{wp} = 3.53 %. Monoclinic $NaCN_3H_4$, Space group 14, *a* = 7.9671(2) Å *b* = 5.0825(2) Å *c* = 9.4202(3) Å β = 110.687(3)°. Orthorhombic NaOH, space group 63, *a* = 3.4061(1) Å *b* = 3. 4061(1) Å *c* = 11.4035(3) Å.

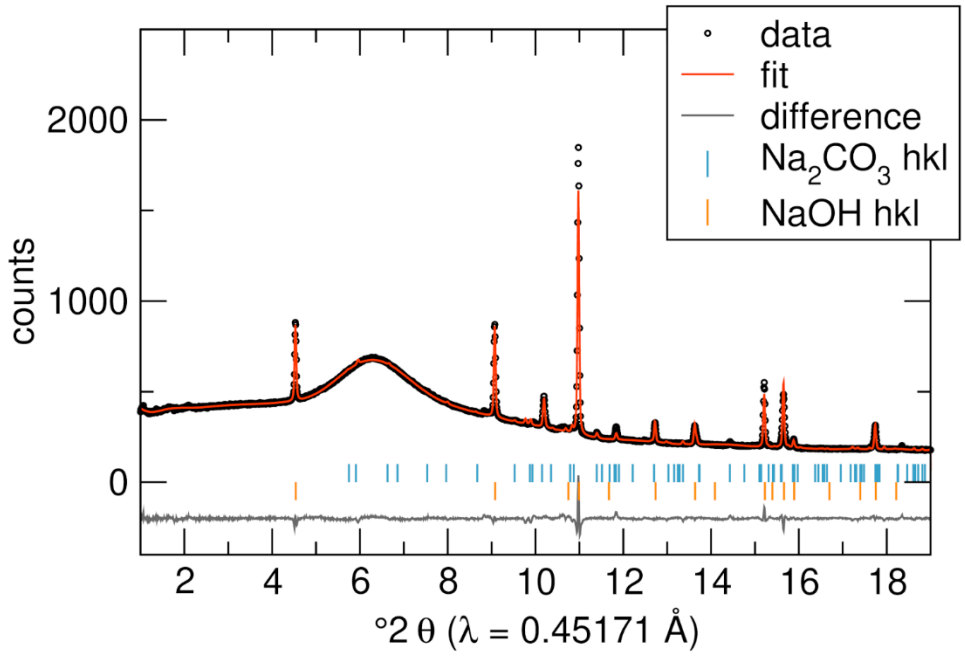

Fig S4. Representative Rietveld refinement fit of X-ray powder diffraction data of $NaCN_3H_4$ under static limited humidity CO_2 after 7 hours, 383 K [APS, 17-BM]. R_{wp} = 2.36 %. Monoclinic Na_2CO_3, Space group 12, *a* = 8.846(1) Å *b* = 5.303(1) Å *c* = 6.099(1) Å β = 100.87(2)°. Orthorhombic NaOH, space group 63, *a* = 3.4124(1) Å *b* = 3.4124(1) Å *c* = 11.4201(4) Å.

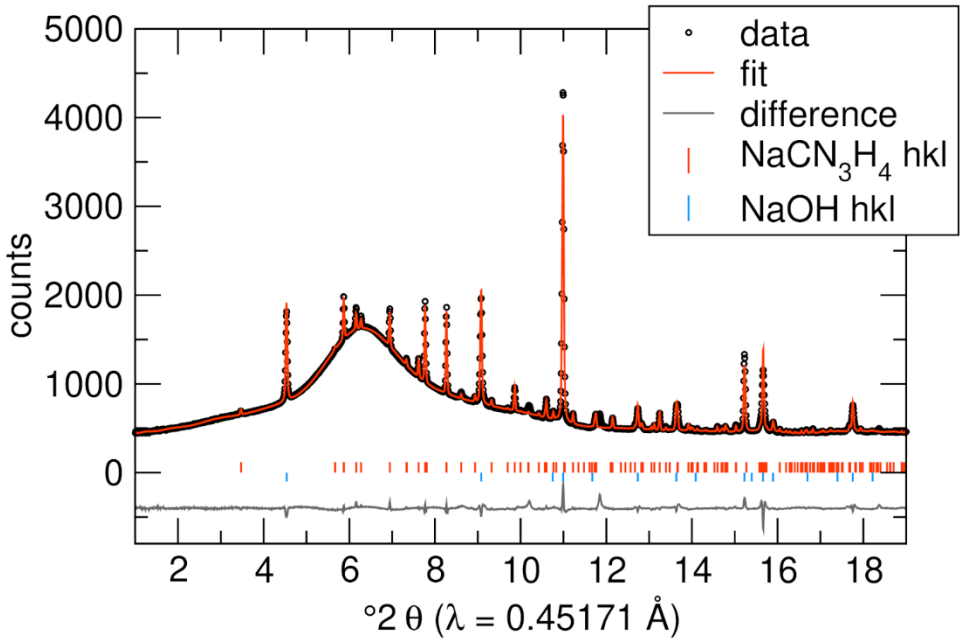

Fig S5. Representative Rietveld refinement fit of X-ray powder diffraction data of $NaCN_3H_4$ under flow limited humidity CO_2 flow after 10 minutes, 350 K [APS, 17-BM]. R_{wp} = 2.32 %. Monoclinic $NaCN_3H_4$, Space group 14, *a* = 7.9681(5) Å *b* = 5.0872(3) Å *c* = 9.4244(6) Å β = 110.669(6)°. Orthorhombic NaOH, space group 63, *a* = 3.4083(1) Å *b* = 3.4083(1) Å *c* = 11.4117(4) Å.

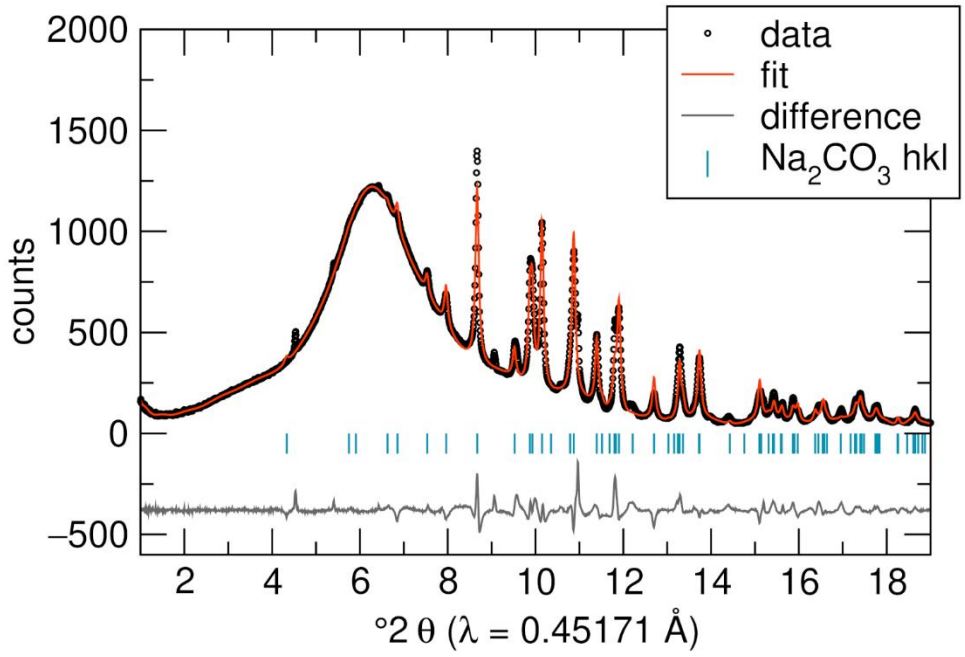

Fig S6. Rietveld refinement fit of X-ray powder diffraction data of $NaCN_3H_4$ under flow limited humidity CO_2 flow after 180 minutes, 383 K [APS, 17-BM]. R_{wp} = 2.98 %. Monoclinic Na_2CO_3, Space group 12, *a* = 8.922(1) Å *b* = 5.2435(7) Å *c* = 6.0788(9) Å β = 100.978(7)°.

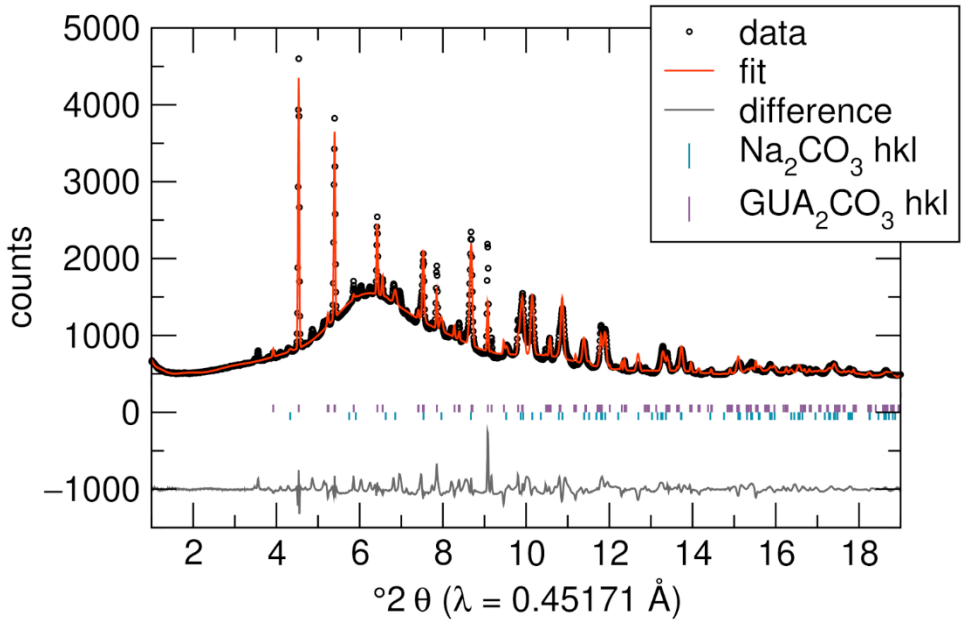

Fig S7. Rietveld refinement fit of X-ray powder diffraction data of $NaCN_3H_4$ under flow limited humidity CO_2 flow after 420 minutes, 383 K [APS, 17-BM]. R_{wp} = 5.68 %. Monoclinic Na_2CO_3, Space group 12, *a* = 8.929(1) Å *b* = 5.253(1) Å *c* = 6.084(1) Å *β* = 100.91(1)°. Orthorhombic guanidinium carbonate (labeled GUA_2CO_3 in Fig.), space group 92, *a* = 7.001(1) Å *b* = 6.996(2) Å *c* = 19.728(3) Å.

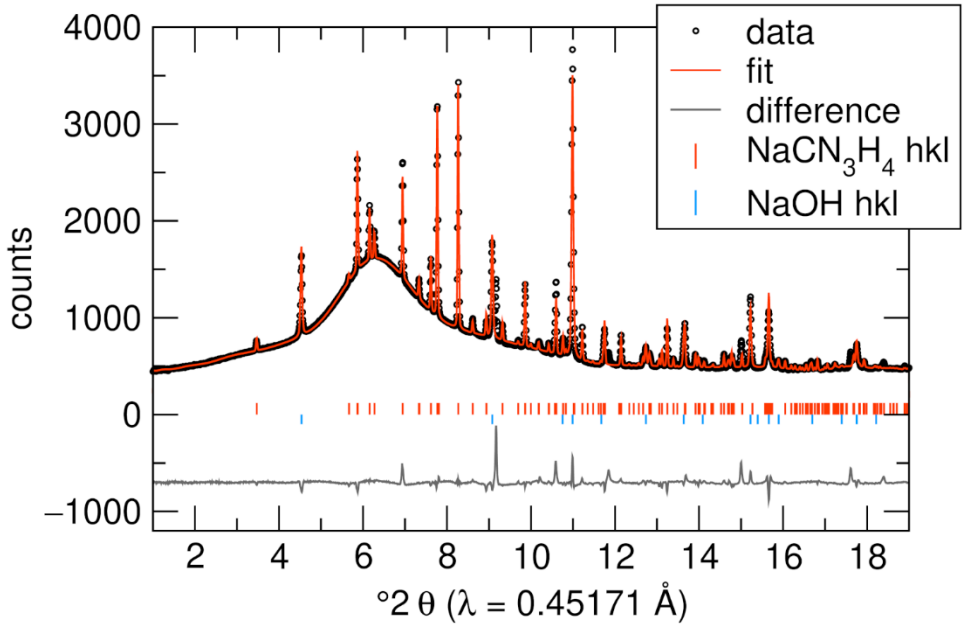

Fig S8. Representative Rietveld refinement fit of X-ray powder diffraction data of $NaCN_3H_4$ under excess humidity CO_2 flow after 10 minutes, 350 K [APS, 17-BM]. R_{wp} = 3.82 %. Monoclinic $NaCN_3H_4$, Space group 14, *a* = 7.9702(3) Å *b* = 5.0888(3) Å *c* = 9.4288(5) Å β = 110.680(4)°. Orthorhombic NaOH, space group 63, *a* = 3.41(1) Å *b* = 3.41(1) Å *c* = 11.4145(5) Å.

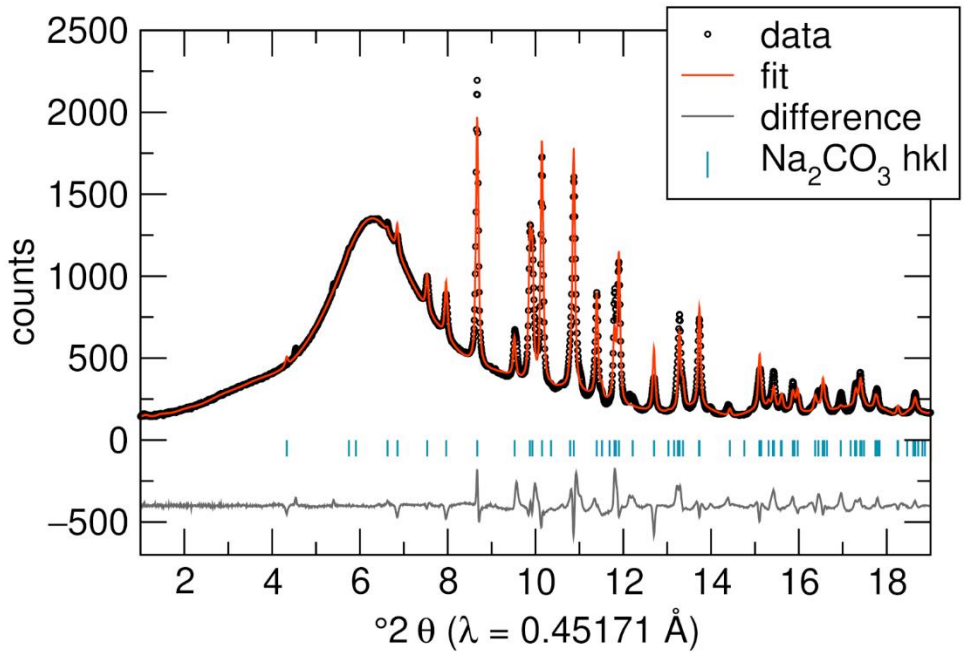

Fig S9. Representative Rietveld refinement fit of X-ray powder diffraction data of $NaCN_3H_4$ under excess humidity CO_2 flow after 50 minutes, 383 K [APS, 17-BM]. R_{wp} = 3.93 %. Monoclinic Na_2CO_3, Space group 12, a = 8.9274(7) Å b = 5.2467(1) Å c = 6.0811(6) Å, β = 100.979(5)°.

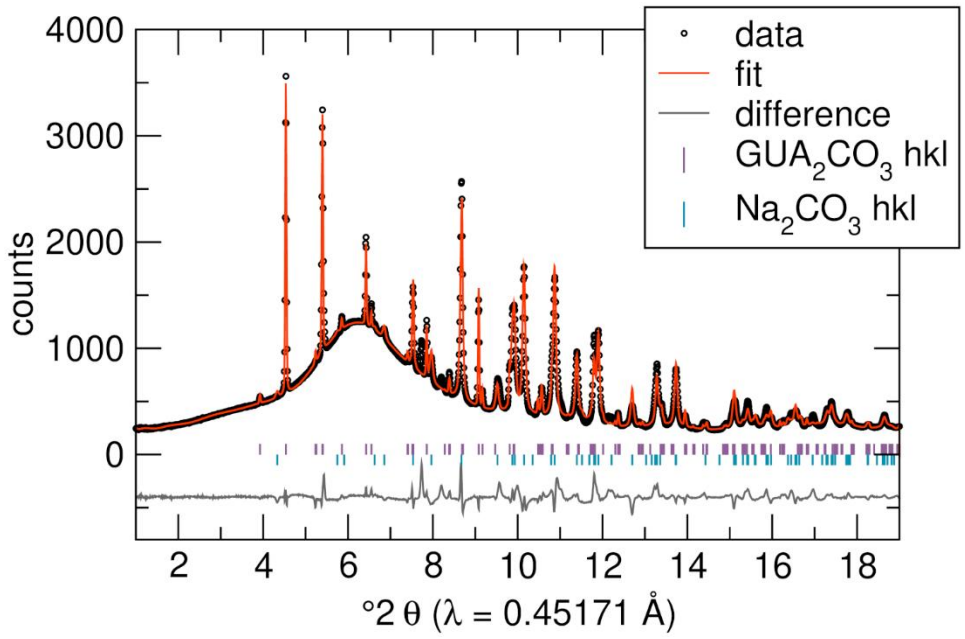

Fig S10. Representative Rietveld refinement fit of X-ray powder diffraction data of $NaCN_3H_4$ under excess humidity CO_2 flow after 200 minutes, 383 K [APS, 17-BM]. R_{wp} = 4.49 %. Monoclinic Na_2CO_3, Space group 12, a = 8.930(1) Å, b = 5.2481(4) Å, c = 6.0842(4) Å, β = 100.977(6)°. Tetragonal guanidinium carbonate (labeled as GUA_2CO_3 in Fig.), space group 92, a = b = 6.996(1), c = 19.5712(2).

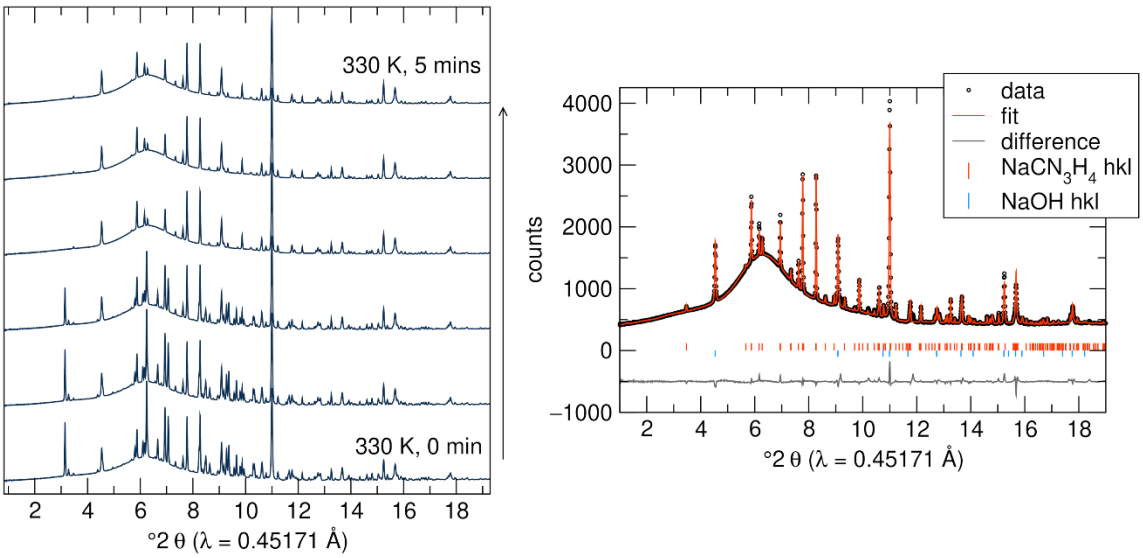

Fig. S11. (left) Unexposed as-made $NaCN_3H_4$ (the mixture of NaH and Guanidine) heated at 330 K to form crystalline $NaCN_3H_4$. (right) Rietveld refinement of the 5-minute data set [APS, 17-BM]. R_{wp} = 2.44 %. Monoclinic $NaCN_3H_4$, Space group 14, *a* = 7.9666(3) Å, *b* = 5.0823(2) Å, *c* = 9.4195(3) Å β = 110.683(3)°. Orthorhombic NaOH, space group 63, *a* = 3.4(2) Å, *b* = 3.4(2) Å, *c* = 11.4005(3) Å.

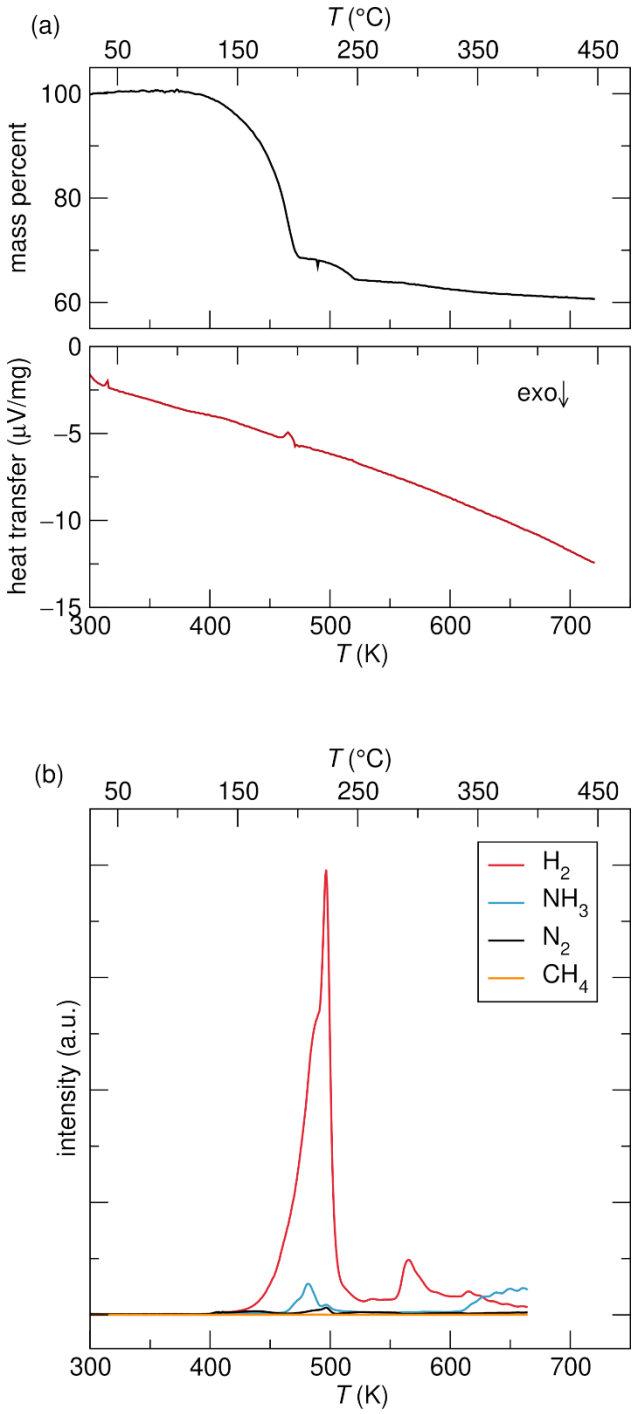

Fig. S12. (a) TGA weight loss, (b) DCS, and (c) mass spectroscopy of $NaCN_3H_4$ with 2 °C/min heating rate to ≈ 723 K (450 °C). $NaCN_3H_4$ under He flow is stable and does not exhibit any exothermic heat event such as amorphization in the studied temperature range 353 K – 388 K (80 °C - 115 °C).

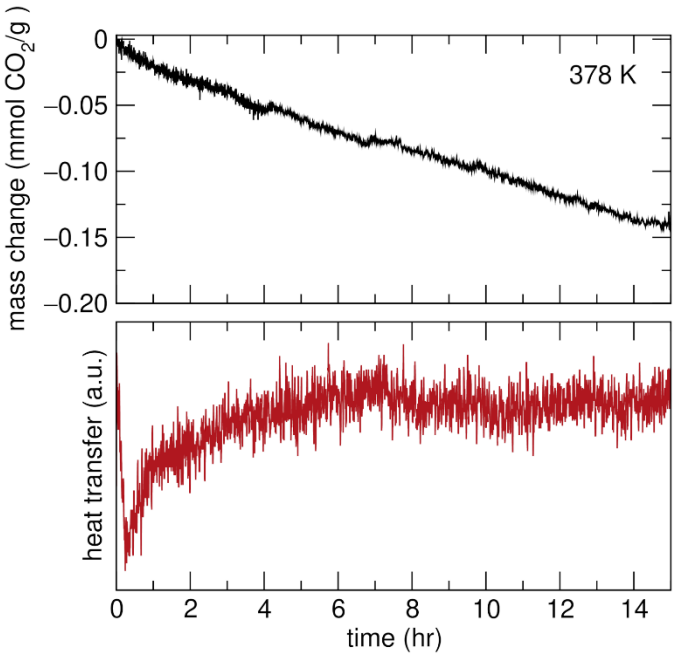

Fig. S13. TGA (top) and DSC (bottom) profiles of $NaCN_3H_4$ under He flow held at 387 K (105°C) and monitored for 15 hours. Mass change has been converted from percent mass change to "mmol/g CO_2" for easy comparison to plots shown in Fig. 3 and Fig. 5 in the main text, even though there is no CO_2 in the system. The graph shows that though there is minor loss of $NaCN_3H_4$ under He gas, it is stable over the prolonged heating at the studied temperature range relative to the mass change observed in Fig. 3 and Fig. 5.

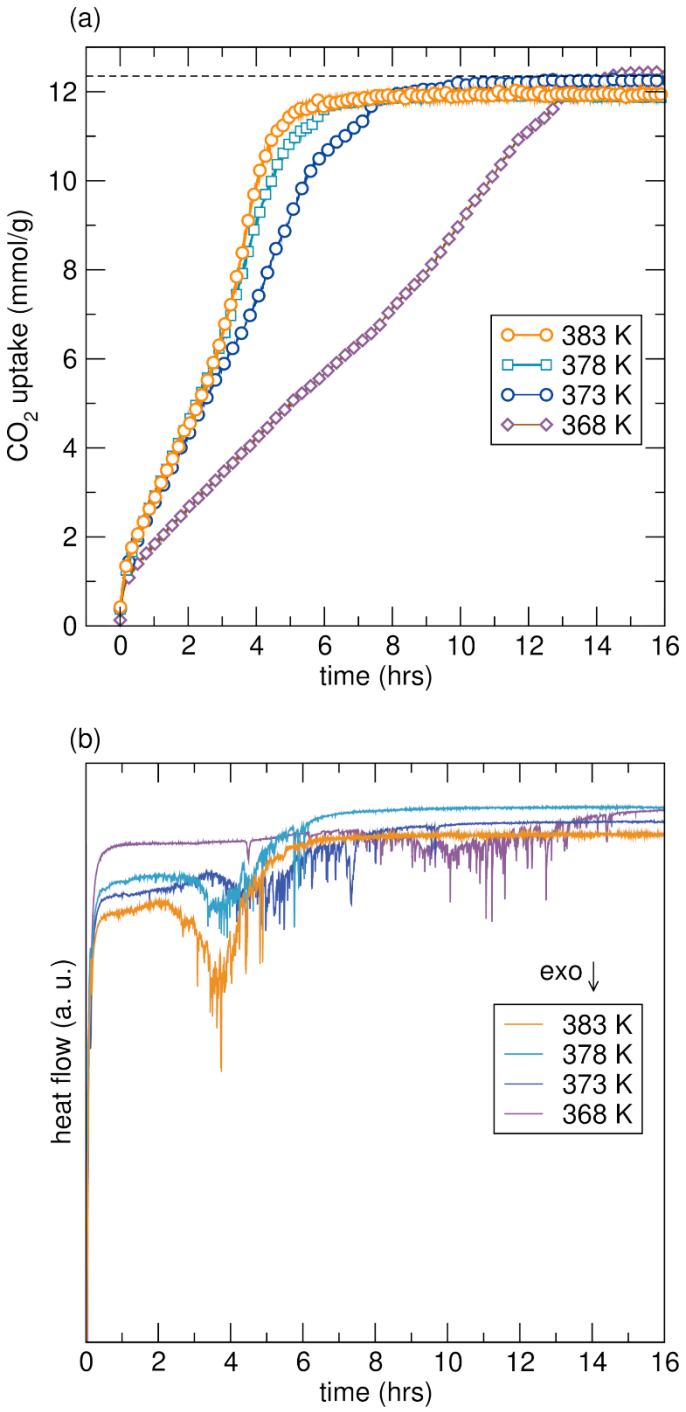

Fig. S14. TGA and DSC results of the wet CO_2 uptake profile at 95°C in comparison with wet CO_2 absorption profiles at ≥ 100°C. We also investigated the wet CO_2 absorption at temperature below 100°C as the sievert experiment indicates that CO_2 absorption can occur at as low as 80°C (Fig.1). The CO_2 uptake rate became significantly slower at 95°C compared to 100°C (Fig. S5). This suggests that temperature, which determines the interfacial diffusion of gases (i.e., H_2O vapor) into bulk solid phase, should be the main external factor affecting the chemisorption rate in the humidity-excess condition.

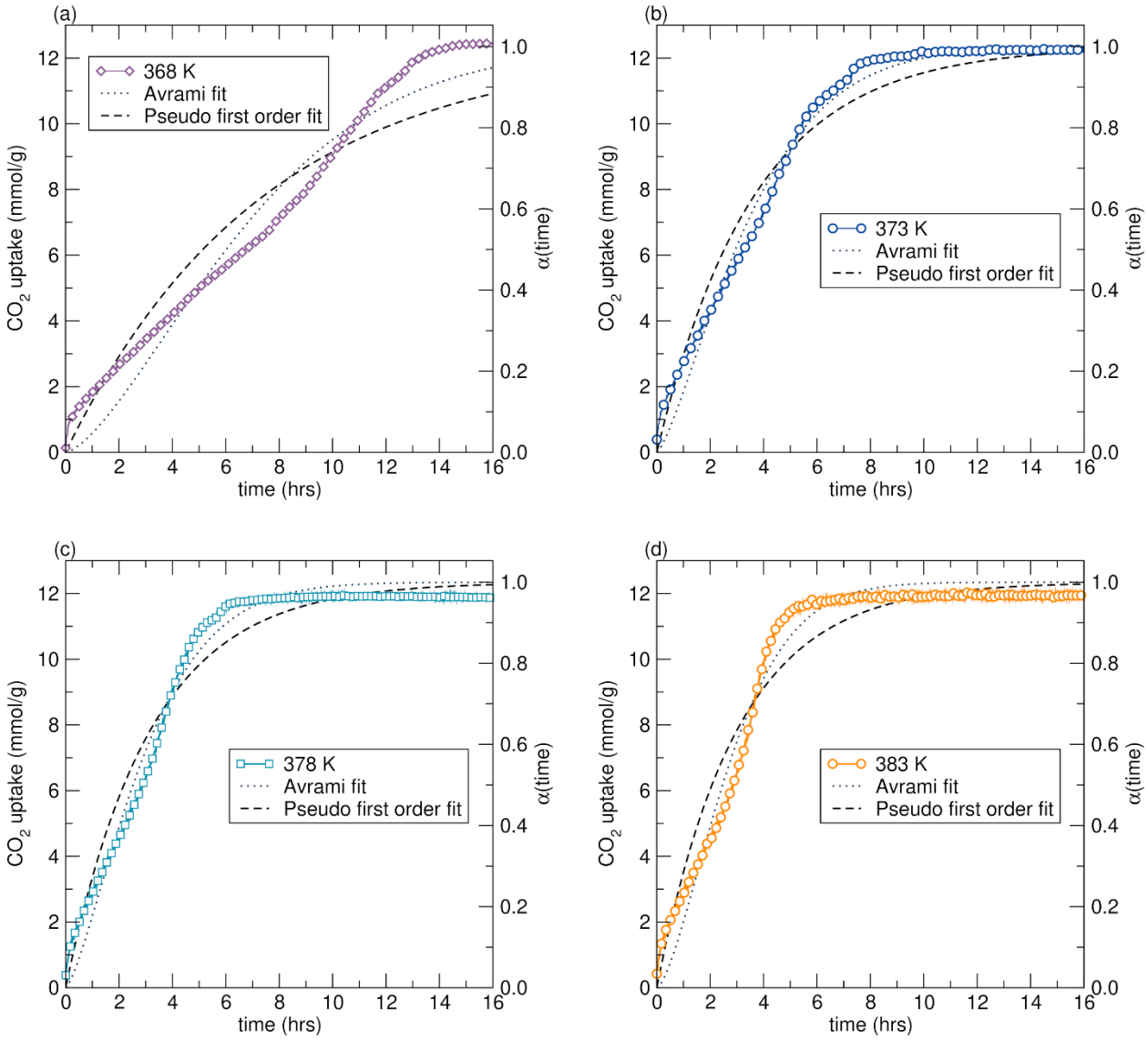

Fig. S15. Humidity-excess TGA CO_2 uptake profiles at different temperatures. The fits of the kinetic data using Pseudo 1st order and Avrami models at each temperature are indicated. The fitting parameters from these two models are summarized in Table S2.

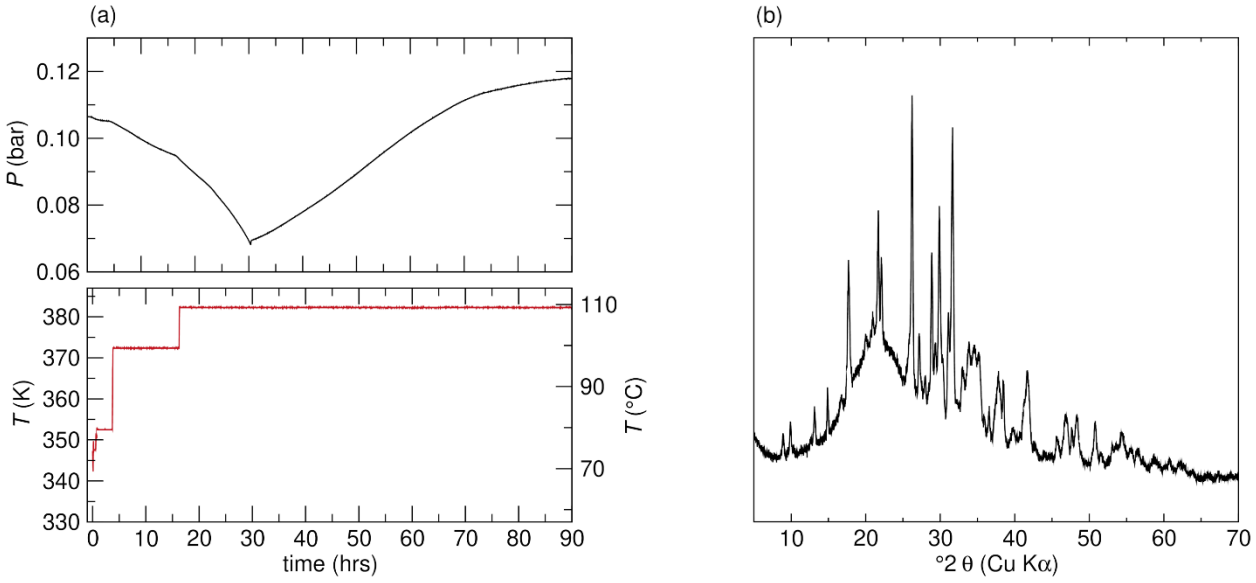

Fig. S16. a) CO_2 absorption change profile with an initial 0.1 bar CO_2 pressure and the tested temperature range of $NaCN_3H_4$. Note: Different from Fig. S1, temperature was kept at 383 K after induction. b) Laboratory PXRD results of the products collected after decomposition. The products are composed of many unknown phases besides Na_2CO_3.

Under the same static humidity-limited condition (as shown in Fig. 1) but with only 0.1 bar CO_2 pressure, we found that after the lengthy induction, the sample will start to decompose and did not undergo a rapid CO_2 absorption, implying the instability of the intermediates at high temperature with the scarce humidity. As discussed in the main text, the rapid absorption stage is dominated by thermodynamic driving force, therefore, the endothermic decomposition of the unstable intermediates can be effectively suppressed by reducing temperature, which meanwhile will not interfere the exothermic carbonation. As demonstrated in Fig. S1, the sample will continue to react with CO_2 after induction at a reduced temperature with the formation of desired $(CN_3H_6)_2CO_3$ and Na_2CO_3.

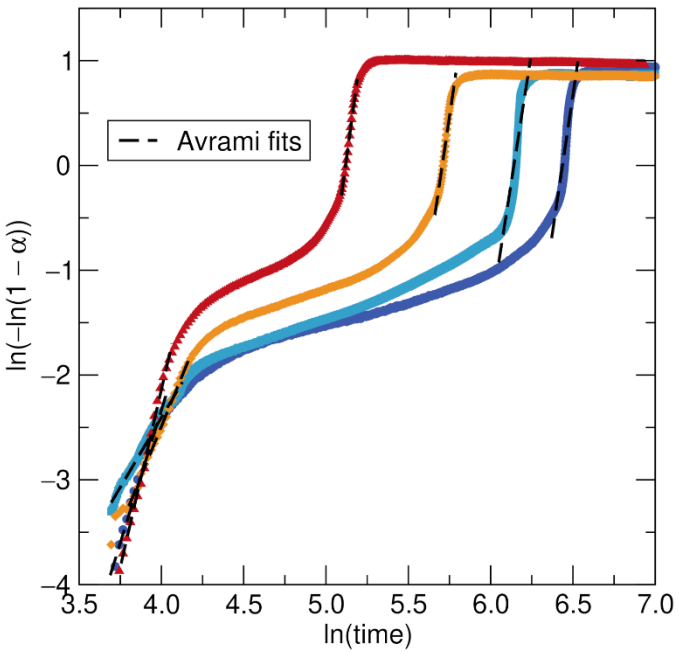

Fig. S17 Avrami fitting to derive Avrami exponents (n) at beginning and late reaction stages of the humidity limited TGA experiments. All values from Avrami fits can be found in Table S1

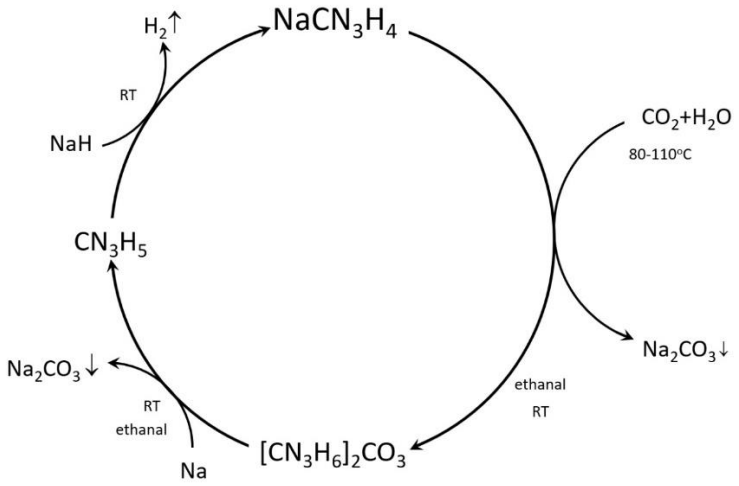

Fig. S18 Proposed carbon capture and regeneration cycle of sodium guanidinate. The merits of such a system include that solid carbonate products i.e., guanidium carbonate and sodium carbonate, can be easily separated in ethanol solution by filtration, and guanidinium carbonate fed back into the system.

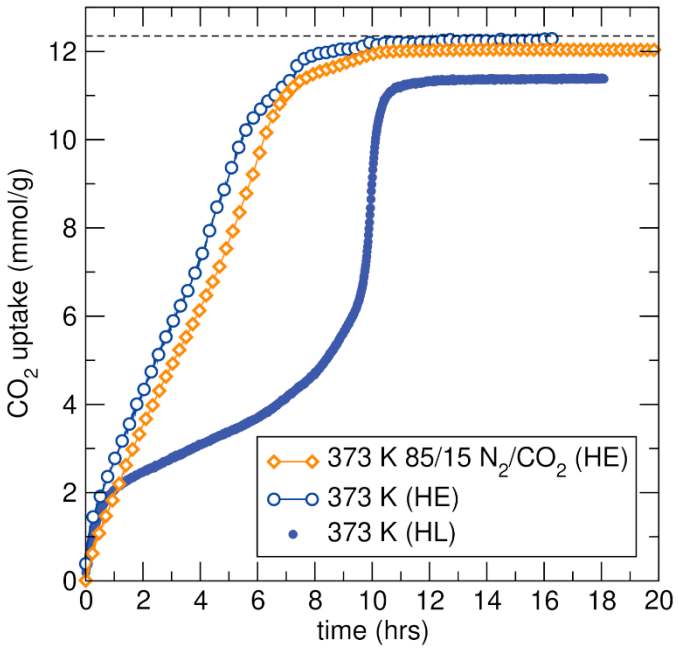

Fig. S19 Flue gas (85/15 N_2/CO_2, humidity excess (HE)) TGA adsorption with $NaCN_3H_4$ at 373 K. For comparison, humidity excess and humidity limited (HL) TGA runs with pure CO_2 are also graphed. The flow rate conditions are the same as was used for the pure CO_2 runs.

Table S1. Avrami kinetic rates (k_A) and exponents (n) at different reaction stages from the fitted lines in Fig. 3 using Avrami equation $\ln \ln \frac{1}{1-\alpha(t)} = n \ln t + n \ln k_A$ for chemisorption under dry CO_2 stream. Reaction Time (min) is the approximate time taken to reach maximum adsorption, not the fitting range. $\alpha(t)$ is the adsorption values normalized to the expected theoretical mmol/g CO_2 adsorption of the reaction, 12.345 mmol/g.

Temp C (K)	Reaction Time (min)	0<α<0.1		0.1<α<0.4-0.5		0.4-0.5<α<1	
		Avrami exponent (n)	k_A	Avrami exponent (n)	k_A	Avrami exponent (n)	k_A
100 (373)	690	4.00	0.01228	0.50	0.000335	10.55	0.00154
105 (378)	510	3.01	0.00798	0.66	0.000760	10.06	0.00217
110 (383)	320	3.84	0.00877	0.61	0.000911	10.61	0.00348
115 (388)	160	6.79	0.01319	0.87	0.00387	11.04	0.00645

Table S2. Fitting parameters from the Avrami kinetic model using equation $\alpha(t)=1\text{-}\exp[-(k_A t)^n]$ and the pseudo 1st order model for chemisorption under wet CO_2 stream. Reaction Time (min) is the approximate time taken to reach maximum adsorption, not the fitting range. $\alpha(t)$ is the adsorption values normalized to the expected theoretical mmol/g CO_2 adsorption of the reaction, 12.345 mmol/g.

Temp °C (K)	Reaction Time (min)	Avrami model			Seudo 1st order model	
		k_A	Avrami exponent (n)	Fitting R^2	k	Fitting R^2
95 (368)	900	0.00216	1.486	0.955	0.00128	0.911
100 (373)	575	0.00431	1.342	0.987	0.00439	0.966
105 (378)	410	0.00506	1.376	0.979	0.00530	0.961
110 (383)	370	0.00530	1.510	0.973	0.00560	0.947

Detailed mechanism description

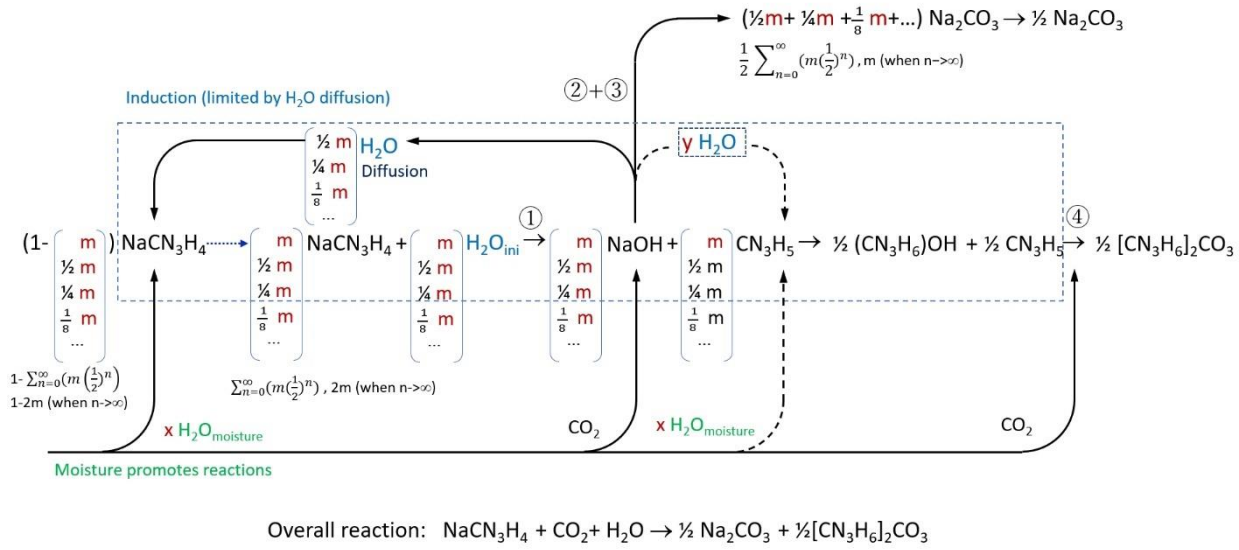

Overall reaction: $NaCN_3H_4 + CO_2 + H_2O \rightarrow ½\ Na_2CO_3 + ½[CN_3H_6]_2CO_3$

Scheme S1. The schematic reaction mechanism for CO_2 capture by $NaCN_3H_4$. The initial H_2O within the sample is indicated as $H2O_{ini}$, the concentration of moisture in the CO_2 stream is indicated by $H_2O(x)$, and the possible amount of H_2O emitted by reaction (2) (3) that also can react with CN_3H_5 is assumed as H_2O (y).

From the evolution of crystalline phases observed from the ex-situ and in-situ XRD studies (main text Fig. 1, 3 and 5), we can deduce a generalized stepwise consecutive CO_2 chemisorption mechanism for $NaCN_3H_4$ as shown in scheme S1 with the following key reactions (1) (2) (3) and (4).

$NaCN_3H_4 + H_2O \rightarrow NaOH + CN_3H_5$. (1)

$NaOH + CO_2 \rightarrow NaHCO_3$ (2)

$NaHCO_3 + NaOH \rightarrow Na_2CO_3 + H_2O$ (3)

$2CN_3H_5 + 2H_2O \rightarrow$ CN_3H_6OH (metastable intermediate) + $CN_3H_5 + CO_2 \rightarrow [CN_3H_6]_2CO_3$ (4)

First, given the highly hygroscopic nature of $NaCN_3H_4$, we assume one unit of $NaCN_3H_4$ can initially scavenge *m* amount of H_2O from the surroundings before they were used for CO_2 absorption. Following reaction (1), this initial H_2O (*m*) inside the sample will contaminate the same amount of $NaCN_3H_4$ (*m*) to form equal amount of neutral guanidine (*m*) and NaOH (*m*) (reaction 1 in scheme 1) and leave remaining (1-*m*) amount of $NaCN_3H_4$ unreacted, which are supported by the initial XRD patterns (Fig. 3 and 5).The *m* amount of NaOH produced could then react with CO_2, following the path of reactions (2) and (3) (also labeled (2)+(3) in scheme S1) with sodium bicarbonate likely forming as an interim intermediate and sodium carbonate as the main reaction product observed in diffraction (Fig. 3 and 5). It should be noted that reactions (2)+(3) will produce (½m) Na_2CO_3 and release (½m) H_2O from *m* NaOH to keep the reaction balanced as shown in Scheme S1.

After the initial round of reactions (1), (2), and (3), the (½ *m*) H_2O released will continue to react with the same amount of $NaCN_3H_4$ (½ *m*) from the remaining (1-*m*) $NaCN_3H_4$, and start the second round of the reactions (1)+(2)+(3), resulting in (½m) CN_3H_5 and (½ *m*)NaOH. The latter will further react with CO_2 and generate (¼ *m*) Na_2CO_3 as well as (¼ *m*) H_2O to infest the rest $NaCN_3H_4$. If such "chain reactions" follow suit, the initial *m* amount of H_2O present in the sample will reacts with totally $m(1+½+¼+\ldots(½)^n)$ $NaCN_3H_4$. The sum of this geometry progression can be written as $\sum_{n=0}^{\infty}(m(\frac{1}{2})^n)$. If the reaction can go infinitely ($n\rightarrow\infty$), the total amount of $NaCN_3H_4$ that can react during the induction period would be 2*m* and the unreacted $NaCN_3H_4$ would be (1-2*m*). To achieve the complete reactions just for the reactions (1)+(2)+(3), *m* should at least be ½, i.e., initial one unit of $NaCN_3H_4$ needs to absorb half of its total amount of H_2O, which is a substantial amount to be initially scavenged by samples handled in a glovebox.

In addition, the freshly formed CN_3H_5 from reaction (1) is highly hygroscopic. Thus it can be speculated that some of the leftover H_2O (y) emitted by reaction (2)(3) (dash black arrowed lines in scheme 1) can also diffuse and react with CN_3H_5 to generate guanidinium hydroxide ($(CN_3H_6)(OH)$) and/or other intermediates. Therefore, in the static humidity-limited condition, CO_2 absorption will be significantly limited by both H_2O related diffusion pathways. For the humidity-limited flow CO_2 condition, from the improved absorption kinetics (main text Fig. 2 and 3), it is reasonable to deduce that the feeding CO_2 must also provide certain amount of H_2O (*x*) to participate in these reactions. Apparently, the *extent* and the *rate* of these reactions can largely be controlled by the humidity level from the feeding CO_2 and the diffusion of H_2O within the samples, which was demonstrated by the extreme case of the CO_2 absorption under the humidity-excess condition (main text Fig. 4 and 5).

.